

Valence electron structures dependences of structural stability and properties of REX_3(*RE*=rare earth; *X*=In, Tl) and $RE(In, Co)_3$ alloys

Boyang Li(李博洋), Yongquan Guo(郭永权), Yi-Chen Feng(冯奕晨), Xinze Wang(王鑫泽), and Wei Liu(刘葳)
Citation: Chin. Phys. B, 2024, 33 (**11**): 116102. DOI: 10.1088/1674-1056/ad7575
Journal homepage: http://cpb.iphy.ac.cn; http://iopscience.iop.org/cpb

What follows is a list of articles you may be interested in

Valence electron structures dependences of structural stability and properties of REX_3(*RE*=rare earth; *X*=In, Tl) and $RE(In, Co)_3$ alloys

Boyang Li(李博洋), Yongquan Guo(郭永权), Yi-Chen Feng(冯奕晨), Xinze Wang(王鑫泽), and Wei Liu(刘葳)
Chin. Phys. B, 2024, 33 (**11**): 116102. DOI: 10.1088/1674-1056/ad7575

Effect of Y element on atomic structure, glass forming ability, and magnetic properties of FeBC alloy

Jin-Hua Xiao(肖晋桦), Da-Wei Ding(丁大伟), Lin Li(李琳), Yi-Tao Sun(孙奕韬), Mao-Zhi Li(李茂枝), and Wei-Hua Wang(汪卫华)
Chin. Phys. B, 2024, 33 (**7**): 076101. DOI: 10.1088/1674-1056/ad3dd4

Geometries and electronic structures of Zr_nCu(*n* =2-12) clusters: A joint machine-learning potential density functional theory investigation

Yizhi Wang(王一志), Xiuhua Cui(崔秀花), Jing Liu(刘静), Qun Jing(井群), Haiming Duan(段海明), and Haibin Cao(曹海宾)
Chin. Phys. B, 2024, 33 (**1**): 016109. DOI: 10.1088/1674-1056/acd5c2

Spin and spin-orbit coupling effects in nickel-based superalloys: A first-principles study on Ni_3Al doped with Ta/W/Re

Liping Liu(刘立平), Jin Cao(曹晋), Wei Guo(郭伟), and Chongyu Wang(王崇愚)
Chin. Phys. B, 2022, 31 (**1**): 016105. DOI: 10.1088/1674-1056/ac4024

Strain-tuned magnetic properties in (Ga,Fe)Sb: First-principles study

Feng-Chun Pan(潘凤春), Xue-Ling Lin(林雪玲), and Xu-Ming Wang(王旭明)
Chin. Phys. B, 2021, 30 (**9**): 096105. DOI: 10.1088/1674-1056/ac00a2

Valence electron structures dependences of structural stability and properties of REX_3 (RE = rare earth; X = In, Tl) and RE(In, Co)$_3$ alloys

Boyang Li(李博洋), Yongquan Guo(郭永权)†, Yi-Chen Feng(冯奕晨), Xinze Wang(王鑫泽), and Wei Liu(刘葳)

School of Energy Power and Mechanical Engineering, North China Electric Power University, Beijing 102206, *China*

(Received 15 May 2024; revised manuscript received 20 August 2024; accepted manuscript online 30 August 2024)

Intermetallic compounds REIn$_3$ (RE = rare earth) have attracted much attention due to their unique characteristics: crystal field effect, Kondo effect, superconductivity, heavy fermion, and antiferromagnetism, and their cobalt diluted alloys exhibit the ferromagnetic half-metallic characteristics at room temperature. In this study, an empirical electron theory (EET) is employed to investigate systemically the valence electronic structure, the thermal and magnetic properties of REX_3 and their cobalt diluted alloys for revealing the mechanism of physical properties. The calculated bond length, melting point, and magnetic moment match the experimental ones very well. The study reveals that structural stability and physical properties of REX_3 and their cobalt dilute alloys are strongly related to their valence electron structures. It is suggested that the structural stability and cohesive energy depend upon the covalent electron, the melting point is modulated by covalent electron pair, and the magnetic moment is originated from 3d magnetic electron. The ferromagnetic characteristics of Co-diluted REIn$_3$ alloys is originated from the introduction of strong ferromagnetic Co atom, but, a competition is caused between the electron transition from valence electron to magnetic electron on d orbit and its reversal electron transformation with increasing the content of cobalt, which results in the formations of diluted magnetic Gd(In,Co)$_3$ alloy with minor amount of cobalt and strong magnetic Nd(In,Co)$_3$ alloy with doping more Co atoms.

Keywords: REX_3, cobalt dilute alloy, valence electron structures, empirical electron theory, moment

PACS: 61.50.Lt, 75.50.–y, 78.40.Kc, 31.10.+z **DOI:** 10.1088/1674-1056/ad7575

1. Introduction

Intermetallic compounds REX_3 (RE = rare earth; X = semimetal In, Ga) with cubic $AuCu_3$-type structure have attracted much attention due to their unique characteristics such as crystal field effect, Kondo effect, multiaxial magnetic structure, superconductivity at critical condition, heavy fermion, and antiferromagnetic characteristics.[1–10] However, the application of REX_3 is limited due to their low magnetic transition temperatures.[1,2,11]

Thus, the addition of 3d transition metals such as Mn, Co is necessary for improving their magnetic properties and realizing room temperature ferromagnetic order. Doping minor amount of 3d transition metal (Fe, Co, or Mn) into REX_3 can be regarded as the diluted magnetic intermetallic compounds (DMIC). Doping Mn into $GdIn_3$ can modulate the magnetic ordered state, and cause the increase of magnetic transition temperature, and doping Mn into $EuGa_3$ leads to form the ferromagnetic order at room temperature under an external field of 40 Oe (1 Oe = 79.5775 A·m^{-1}).[12] The similar phenomenon is also observed in Co-doped $HoIn_{3-x}Co_x$.[13] The addition of 3d transition metal into an alloy or an intermetallic compound not only enhances magnetic moments, but also improves the magnetic anisotropy by the exchange coupling interaction between 3d electrons of transition metals and 4f electrons of rare earths.[14–16]

Theorical calculation is necessary for predicting the physical properties, such as quantum anomalous,[17] thermal conductivity,[18] phase transition,[19] etc. REX_3 intermetallic compounds are theoretically studied with some approaches and models such as the first principle and semi-empirical models. The full-potential linearized augmented plane wave (FLAPW) based on the density functional theory (DFT), which is built based on the first-principle, has been used to study the energy-band structures of some REX_3 intermetallic compounds. The theoretical studies also cover the energy spectrum of electron, angle dependence of the cyclotron masses, and elastic & electronic properties.[20–23]

The empirical electron theory (EET) has been successfully applied to study the physical properties of solids and molecules, including the mechanical properties (such as stress, strain, and elastic modulus), thermal properties (melting point, cohesion energy, and thermal conductivity), electric and magnetic properties (magnetic moment, electron conductivity, and Curie temperature), and EET is also used to calculate the binary phase diagrams of alloys and compounds. In this study, EET is used to study systematically the valence electron structures, melting point, cohesive energy, and magnetic moment of the REX_3 intermetallic compounds and their cobalt dilute alloys in order to reveal the correlation between their valence electron structures and physical properties.

†Corresponding author. E-mail: yqguo@ncepu.edu.cn

© 2024 Chinese Physical Society and IOP Publishing Ltd

2. Model formulation

EET, which is consisted by three basic hypotheses and a calculation method, is used for determining the valence electron structures of alloys and compounds, and calculating their multiple physical properties.[24–26]

Hypothesis 1 In solid and molecule, each atom is generally hybridized by two atomic states, which are so-called h and t, respectively, one of them is in the excited state or near to the ground state. The hybrid state is consisted by various electrons (valence electron, lattice electron, 3d magnetic electron, and dumb-pair electron) and single-bond radius $R(1)$.

Hypothesis 2 The hybrid states of atoms are discontinuous, which can be calculated by the weighted average of state proportions of h and t states with K-equation as listed in the supporting information. The hybrid table can be built based on the first two hypotheses, which cover all of hybrid states with various electrons and single-bond radius.

Hypothesis 3 The covalent bond length between atoms u and v is calculated according to the number of covalent electron pairs n_α and single-bond radii, as given below:

$$D_{uv}(n_\alpha) = R_u(1) + R_v(1) - \beta \log n_\alpha \quad (\alpha = A, B, C, \ldots, N), \tag{1}$$

where $R_u(1)$ and $R_v(1)$ denote the single-bond radii of u and v atoms, respectively. n_α denotes the number of covalence electron pairs on the α-th bond, and the parameter β can reflect the overlap-ability of the electron clouds between the u and v atoms.

The bond length difference (BLD) method is used to determine the valence electron structures for all elements in one structural formula by solving n kinds of theoretical bond lengths with the bond equation in hypothesis 3. The hybrid states of all elements can be determined by a criterion of bond length difference of the experiment and calculation ΔD less than 0.05 Å under the first-order approximation. The detailed information is supplied in the supporting information.

2.1. Models of cohesive energy and melting point

The physical model of cohesive energy is built based on the parameters of valence electron structures, which consists of the bonding energy, electric potential, magnetic potential, and condensing energy, as given below:[27–29]

$$E_c = \sum_\alpha \frac{b_\alpha I_\alpha n_\alpha}{\overline{D_\alpha}} f_\alpha + \frac{b_l \sum n_l}{\overline{D}} f' + \sum_i b_i a m_i^{3d} - \sum_i b_i C_i W_i. \tag{2}$$

The model of melting point is built on an assumption of the strongest bond broken by heat vibration energy at the critical temperature (melting point). As long as the vibrating energy of thermal phonon just equals the bonding energy of the strongest bond, the strongest bond is broken by the vibration of the thermal phonon, and the other bonds are also simultaneously broken, which lead to the collapse of the structural skeleton, and induce a phase transition from solid to liquid state. The solid state structure is melting.[27,29,30] The bond energy of the strongest bond can be estimated by

$$U_B = b \frac{n_A}{\overline{D_A}} f + b_l \frac{n_l}{I^\sigma \overline{D}} f' - \frac{\sum b_i C_i W_i}{I^\sigma}. \tag{3}$$

The vibrating energy of thermal phonon with n mole is $1.5nRT$. At the melting point (T_m), the vibrating energy just equals the energy of the strongest bond, i.e., $1.5nRT_m = U_B$. Therefore, the melting point can be calculated as follows:

$$T_m = \left(b \frac{n_A}{\overline{D_A}} f + b_l \frac{n_l}{I^\sigma \overline{D}} f' - \frac{\sum b_i C_i W_i}{I^\sigma} \right) \Big/ \left(\frac{3}{2} nR\right), \tag{4}$$

The detailed information is supplied in the supporting information.

2.2. Model of magnetic moment

According to the criterion of $\Delta D \leq 0.05$ Å in the BLD method, the hybridization states of atoms in a structural formula can be determined, and the state proportions of $C_{h\sigma}$ and $C_{t\sigma}$ are also determined.

The atomic magnetic moment can be estimated by the weight sum of 3d magnetic electron numbers in h and t states as given below:[28,29]

$$m^{3d} = C_{h\sigma} m_h^{3d} + C_{t\sigma} m_t^{3d}. \tag{5}$$

For a structural formula, then we have

$$m^{3d} = \sum_i^N m_i^{3d} A_i, \tag{6}$$

where A_i and m_i^{3d} denote the atomic number of the i-th atom and its 3d magnetic electron number.

2.3. Result and discussion

2.4. REX_3 (RE = rare earth metals; X = In, Tl) intermetallic compounds

REX_3 has a cubic $AuCu_3$-type structure with a space group of $Pm\bar{3}m$, as shown in Fig. 1. The experimental bond lengths can be measured with a diamond software according to the atomic ordinates in report.[31] The calculated bond lengths match the experimental ones well, as listed in Table 1. It is suggested that RE–X bond significant contributes to the structural stability of REX_3 since its number of covalence electron pair n_A is the largest among all bonds in a unit cell in REX_3. For $RE\text{In}_3$ intermetallic compounds, n_A is in an range from 0.2527 to 0.3395. However, n_A decreases significantly to the range of 0.2240–0.2495 in $RE\text{Tl}_3$, which is due to the change of parameter β from 0.60 in $RE\text{In}_3$ to 0.71 in $RE\text{Tl}_3$. It is suggested that the bonding interaction of Tl and RE enhances the overlap ability of electron clouds on RE–Tl bond. The valence

electron structures of *RE* and *X* atoms, which include the distributions of various valence electrons and single-bond radii, are listed in Table 2. In *LRE*In$_3$ (*LRE* = light rare earth), the hybrid states are on the 7-th ($\sigma = 7$) level for *LRE* and the 6-th ($\sigma = 6$) level for In, respectively. However, the single-bond radius of *LRE* decreases with increasing atomic order number from La to Sm, this phenomenon is similar to the shrinking effect of atomic radius in lanthanum system. Figure 1(a) shows the parameter of β lightly increases with the decrease of single-bond radius, which is helpful for enhancing the overlap ability of electron cloudy on *LRE*-In bond. The single-bond radius shows abnormal decrease from 1.6104 for Sm to 1.4127 for heavy rare earth Gd, it might be due to the special electron-arrangement of Gd on 4f orbit since the electron numbers of Gd are more than half of full 4f electron numbers. The electron shielding effect is enhanced and causes the significant declination of radius. The abnormal decrease of single-bond radius induces the transitions of hybrid states from the 6-th ($\sigma = 6$) for light rare earth *LRE* to the 2nd ($\sigma = 2$) hybrid level for the heavy rare earth (*HRE*), and from the 7th ($\sigma = 7$) for In in *LRE*In$_3$ to the 8-th ($\sigma = 8$) hybrid level for In in *HRE*In$_3$. This phenomenon is suggested to be due to the electron transformation from valence electron to lattice electron, the number of s valence electrons n_s decrease from 0.3751 to 0.0365, but, the lattice electron n_l increase from 0.6249 to 0.9635 for *RE*, which induces the significant decrease of covalence electron numbers from 2.3751 to 2.0365. However, a reversal electron transformation from lattice electron to valence electron occurs for In, meanwhile, it is also associated with an additional transition from dumb-pair electron to valence electron, and causes the increase of covalence electron number of In atom.

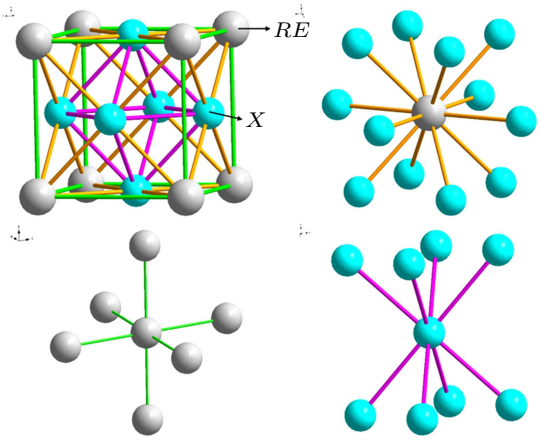


Fig. 1. Crystal structural frame of REX_3.

Table 1. The valence bond lengths and numbers of covalent electron pairs n_α.

Compounds	T_m (cal)	T_m (exp)	I_α	Bonds	D (Å) (exp)	$\bar{D}$ (Å) (Cal)	ΔD (Å)	n_α
$LaIn_3$	1496	1413[32]	24	La–In	3.3480	3.3844	0.03641	0.3076
			24	In–In	3.3480	3.3844	0.03641	0.1301
			6	La–La	4.7350	4.7714	0.03641	0.0036
$CeIn_3$	1483	1453[32]	24	Ce–In	3.3156	3.3488	0.06318	0.3047
			24	In–In	3.3156	3.3488	0.06318	0.1329
			6	Ce–Ce	4.6890	4.7222	0.06318	0.0036
$PrIn_3$	1473	1483[32]	24	Pr–In	3.3036	3.3732	0.06960	0.3018
			24	In–In	3.3036	3.3732	0.06960	0.1358
			6	Pr–Pr	4.6720	4.7416	0.06960	0.0035
$NdIn_3$	1459	1493[32]	24	Nd–In	3.2916	3.3697	0.07821	0.2985
			24	In–In	3.2916	3.3697	0.07821	0.1391
			6	Nd–Nd	4.6550	4.7332	0.07821	0.0035
$SmIn_3$	1420	1403[32]	24	Sm–In	3.2711	3.3698	0.09872	0.2907
			24	In–In	3.2711	3.3698	0.09872	0.1469
			6	Sm–Sm	4.6260	4.7247	0.09872	0.0038
$GdIn_3$	1457	1448[32]	24	Gd–In	3.2576	3.2452	0.01279	0.2789
			24	In–In	3.2576	3.2452	0.01279	0.2242
			6	Gd–Gd	4.6070	4.5942	0.01279	0.0028
$TbIn_3$	1435	1413[32]	24	Tb–In	3.2456	3.2459	0.00009	0.2750
			24	In–In	3.2456	3.2459	0.00009	0.2281
			6	Tb–Tb	4.5900	4.5899	0.00009	0.0029
$DyIn_3$	1416	1423[32]	24	Dy–In	3.2378	3.2465	0.00854	0.2712
			24	In–In	3.2378	3.2465	0.00854	0.2319
			6	Dy–Dy	4.5790	4.5875	0.00854	0.0030
$HoIn_3$	1396	1403[32]	24	Ho-In	3.2336	3.2471	0.01410	0.2675
			24	In–In	3.2336	3.2471	0.01410	0.2355
			6	Ho–Ho	4.5730	4.5871	0.01410	0.0031
$ErIn_3$	1378	1363[32]	24	Er–In	3.2272	3.2476	0.02062	0.2639
			24	In–In	3.2272	3.2476	0.02062	0.2391
			6	Er–Er	4.5640	4.5846	0.02062	0.0031

Table 1. (*Continued*).

Compounds	T_m (cal)	T_m (exp)	I_α	Bonds	D (Å) (exp)	$\bar{D}$ (Å) (Cal)	ΔD (Å)	n_α
$TmIn_3$	1359	1333[32]	24	Tm–In	3.2230	3.2481	0.02509	0.2604
			24	In–In	3.2230	3.2481	0.02509	0.2426
			6	Tm–Tm	4.5580	4.5831	0.02509	0.0032
$YbIn_3$	979	903[32]	24	Yb–In	3.2630	3.3310	0.06803	0.2116
			24	In–In	3.2630	3.3310	0.06803	0.2122
			6	Yb–Yb	4.6150	4.6830	0.06803	0.0026
$LuIn_3$	1321	1236[32]	24	Lu–In	3.2190	3.2490	0.02997	0.2527
			24	In–In	3.2190	3.2490	0.02997	0.2503
			6	Lu–Lu	4.5530	4.5830	0.02997	0.0033
$LaTl_3$	1240	1333[33]	24	La–Tl	3.3984	3.3963	–0.00206	0.2495
			24	Tl–Tl	3.3984	3.3963	–0.00206	0.1305
			6	La–La	4.8060	4.8039	–0.00206	0.0031
$CeTl_3$	1239	1338[33]	24	Ce–Tl	3.3708	3.4027	0.03191	0.2482
			24	Tl–Tl	3.3708	3.4027	0.03191	0.1332
			6	Ce–Ce	4.7670	4.7989	0.03191	0.0033
$PrTl_3$	1227	1338[33]	24	Pr–Tl	3.3566	3.3857	0.02912	0.2450
			24	Tl–Tl	3.3566	3.3857	0.02912	0.1350
			6	Pr–Pr	4.7470	4.7761	0.02912	0.0031
$NdTl_3$	1222	1263[33]	24	Nd–Tl	3.3467	3.3922	0.04555	0.2437
			24	Tl–Tl	3.3467	3.3922	0.04555	0.1378
			6	Nd–Nd	4.7330	4.7785	0.04555	0.0032
$GdTl_3$	1181	1213[33]	24	Dg–Tl	3.3163	3.3602	0.04396	0.2335
			24	Tl–Tl	3.3163	3.3602	0.04396	0.1466
			6	Gd–Gd	4.6900	4.7339	0.04396	0.0027
$TbTl_3$	1171	1213[33]	24	Tb–Tl	3.3093	3.3554	0.04615	0.2311
			24	Tl–Tl	3.3093	3.3554	0.04615	0.1489
			6	Tb–Tb	4.6800	4.7261	0.04615	0.0027
$DyTl_3$	1161	1183[33]	24	Dy–Tl	3.3036	3.3504	0.04687	0.2288
			24	Tl–Tl	3.3036	3.3504	0.04687	0.1513
			6	Dy–Dy	4.6720	4.7188	0.04687	0.0026
$HoTl_3$	1150	1123[33]	24	Ho–Tl	3.2994	3.3457	0.04632	0.2264
			24	Tl–Tl	3.2994	3.3457	0.04632	0.1537
			6	Ho–Ho	4.666	4.7123	0.04632	0.0025
$ErTl_3$	1140	1880[33]	24	Er–Tl	3.2958	3.3408	0.04503	0.2240
			24	Tl–Tl	3.2958	3.3408	0.04503	0.1561
			6	Er–Er	4.6610	4.7060	0.04503	0.0024

Table 2. Numbers of various valence electrons and single-bond radii of REX_3 compounds.

REX_3	Atom	σ	n_l	n_c	n_s	n_p	n_d	m^{3d}	n_{dumb}	$R(1)$
$LaIn_3$	La	6	0.6249	2.3751	0.3751	0.6249	1.3751	0	0	1.6507
	In	7	0.7612	2.7165	0.2388	0.2388	0.2388	0	9.5224	1.4265
$CeIn_3$	Ce	6	0.6249	2.3751	0.3751	0.6249	1.3751	0	0	1.6426
	In	7	0.7612	2.7165	0.2388	0.2388	0.2388	0	9.5224	1.4265
$PrIn_3$	Pr	6	0.6249	2.3751	0.3751	0.6249	1.3751	0	0	1.6346
	In	7	0.7612	2.7165	0.2388	0.2388	0.2388	0	9.5224	1.4265
$NdIn_3$	Nd	6	0.6249	2.3751	0.3751	0.6249	1.3751	0	0	1.6265
	In	7	0.7612	2.7165	0.2388	0.2388	0.2388	0	9.5224	1.4265
$SmIn_3$	Sm	6	0.6249	2.3751	0.3751	0.6249	1.3751	0	0	1.6104
	In	7	0.7612	2.7165	0.2388	0.2388	0.2388	0	9.5224	1.4127
$GdIn_3$	Gd	2	0.9635	2.0365	0.0365	0.9635	1.0365	0	0	1.4740
	In	8	0.5495	3.3516	0.4505	2.4505	0.4505	0	9.099	1.4127
$TbIn_3$	Tb	2	0.9635	2.0365	0.0365	0.9635	1.0365	0	0	1.4660
	In	8	0.5495	3.3516	0.4505	2.4505	0.4505	0	9.0990	1.4127
$DyIn_3$	Dy	2	0.9635	2.0365	0.0365	0.9635	1.0365	0	0	1.4579
	In	8	0.5495	3.3516	0.4505	2.4505	0.4505	0	9.0990	1.4127
$HoIn_3$	Ho	2	0.9635	2.0365	0.0365	0.9635	1.0365	0	0	1.4499
	In	8	0.5495	3.3516	0.4505	2.4505	0.4505	0	9.0990	1.4127
$ErIn_3$	Er	2	0.9635	2.0365	0.0365	0.9635	1.0365	0	0	1.4418
	In	8	0.5495	3.3516	0.4505	2.4505	0.4505	0	9.0990	1.4127

Table 2. (*Continued*).

REX_3	Atom	σ	n_l	n_c	n_s	n_p	n_d	m^{3d}	n_{dumb}	$R(1)$
$TmIn_3$	Tm	2	0.9635	2.0365	0.0365	0.9635	1.0365	0	0	1.4338
	In	8	0.5495	3.3516	0.4505	2.4505	0.4505	0	9.0990	1.4127
$YbIn_3$	Yb	2	0.9635	2.0365	0.0365	0.9635	1.0365	0	0	1.4257
	In	7	0.7271	2.7165	0.2388	2.2388	0.2388	0	9.5224	1.4265
$LuIn_3$	Lu	2	0.9635	2.0365	0.0365	0.9635	1.0365	0	0	1.5541
	In	8	0.5495	3.3516	0.4505	2.4505	0.4505	0	9.0990	1.4127
$LaTl_3$	La	1	1	2	0	1	1	0	0	1.5174
	Tl	6	0.8735	2.3793	0.1264	2.1264	0.1264	0	9.7471	1.4508
$CeTl_3$	Ce	2	0.9635	2.0364	0.03645	0.9635	1.0364	0	0	1.5223
	Tl	6	0.8735	2.3793	0.1264	2.1264	0.1264	0	9.7471	1.4508
$PrTl_3$	Pr	1	1	2	0	1	1	0	0	1.5013
	Tl	6	0.8735	2.3793	0.1264	2.1264	0.1264	0	9.7471	1.4508
$NdTl_3$	Nd	2	0.9635	2.0364	0.03645	0.9635	1.0364	0	0	1.5062
	Tl	6	0.8735	2.3793	0.1264	2.1264	0.1264	0	9.7471	1.4508
$GdTl_3$	Gd	1	1	2	0	1	1	0	0	1.4610
	Tl	6	0.8735	2.3793	0.1264	2.1264	0.1264	0	9.7471	1.4508
$TbTl_3$	Tb	1	1	2	0	1	1	0	0	1.4530
	Tl	6	0.8735	2.3793	0.1264	2.1264	0.1264	0	9.7471	1.4508
$DyTl_3$	Dy	1	1	2	0	1	1	0	0	1.4449
	Tl	6	0.8735	2.3793	0.1264	2.1264	0.1264	0	9.7471	1.4508
$HoTl_3$	Ho	1	1	2	0	1	1	0	0	1.4369
	Tl	6	0.8735	2.3793	0.1264	2.1264	0.1264	0	9.7471	1.4508
$ErTl_3$	Er	1	1	2	0	1	1	0	0	1.4288
	Tl	6	0.8735	2.3793	0.1264	2.1264	0.1264	0	9.7471	1.4508

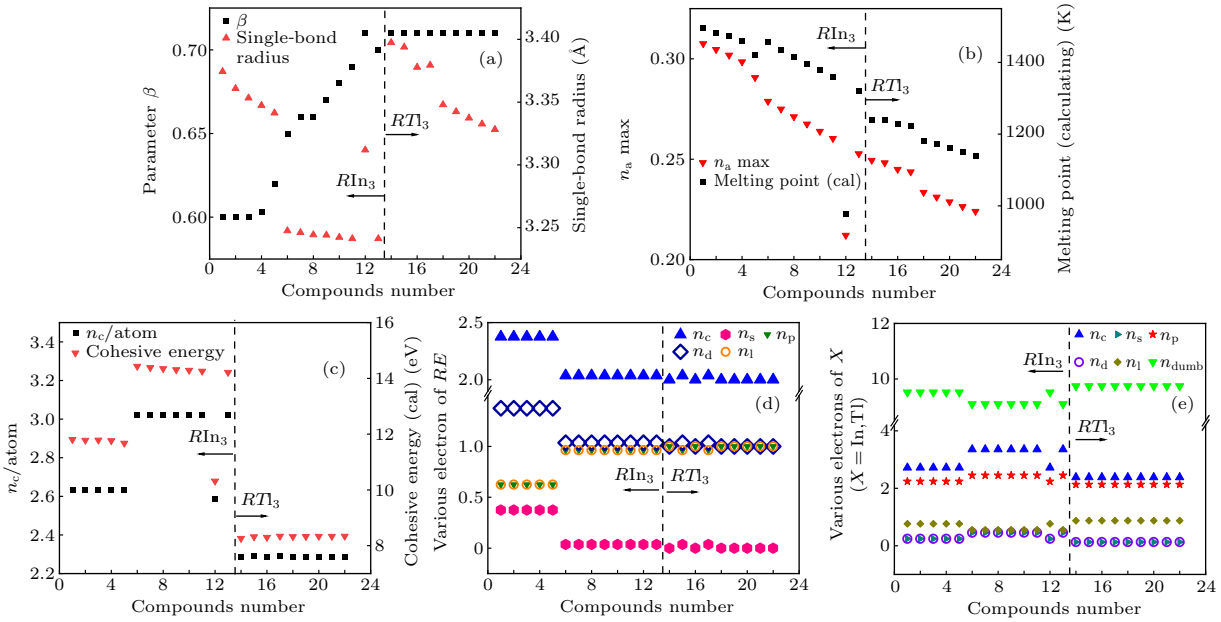


Fig. 2. The correlation of valence electron structure and melting point and cohesive energy of REX_3, where the series orders of $REIn_3$ intermetallic compounds. 1: $LaIn_3$, 2: $CeIn_3$, 3: $PrIn_3$, 4: $NdIn_3$, 5: $SmIn_3$, 6: $GdIn_3$, 7: $TbIn_3$, 8: $DyIn_3$, 9: $HoIn_3$, 10: $ErIn_3$, 11: $TmIn_3$, 12: $YbIn_3$, 13: $LuIn_3$, 14: $LaTl_3$, 15: $CeTl_3$, 16: $PrTl_3$, 17: $NdTl_3$, 18: $GdTl_3$, 19: $TbTl_3$, 20: $DyTl_3$, 21: $HoTl_3$. (a) The single-bond radius dependence of parameter β for REX_3. (b) The melting points and covalence electron pairs of REX_3. (c) The cohesive energies and covalence electrons of REX_3. (d) The covalence, lattice, and s, p, d orbits electrons of RE in REX_3. (e) The covalence, lattice, dumb-pair, and s, p, d orbits electrons of X in REX_3.

In $RETl_3$, all hybrid levels of RE except for Ce and Nd are in the ground state (h state, $\sigma = 1$), the hybrid states of Ce and Nd are on the 2-nd level, which is due to the electron transitions from valence electron to lattice electron on s orbit and dumb-pair electron on d orbit. The hybrid level of Tl is in the 8-th hybrid state. Figure 2(b) shows the strong correlation between the cohesive energy and covalence electron n_c, the cohesive energies of REX_3 strongly depend upon their n_cs, and

arise with the increase of n_c. Since the high cohesive energy is beneficial for the structural stability, it is suggested that increase of n_c can stabilize the crystal structure of REX_3. Thus, REIn$_3$ is more stable than RETl$_3$ since its covalence electron number is more than that of RETi$_3$. In REIn$_3$, the structural ability of HREIn$_3$ is more than that of LREIn$_3$. The calculated melting points of REX_3 agree with the measured ones in binary phase diagrams.[32,33] The calculated results reveal that melting point is strongly related to the maximum number of covalence electron pair n_A, as shown in Fig. 2(c), and arises with increase of n_A. The melting point of REIn$_3$ is higher than that of RETl$_3$, which is due to its large n_A. For REIn$_3$, the melting point shows the same tendency as that of the cohesive energy. n_A decreases with increasing the number of atomic order in lanthanum system. However, the melting point of YbIn$_3$ is abnormally lower than these of the other REIn$_3$. This phenomenon can be explained by the electron transformations from valence electrons to dumb-pair and lattice electrons in In atom, which is induced by the abnormal expansion of bond-length of Yb–In driven by increase of hybrid level of In atom from the 7-th to the 8-th level. Figures 2(d)–2(e) show the changes of covalence and lattice electrons for RE and X. The change tendency of covalence electrons is reversal to that of lattice electrons, since the total numbers of covalence and lattice electrons are 3 for RE, which verifies the mutual electron transformation between covalence and lattice electron in RE. For In atom, the electron transformations are not only from lattice electron n_l to the s valence electron n_s on s orbit, but also from the one dumb-pair n_{s-p} on d orbit to p and d valence electrons. However, RETl$_3$ occurs the reversal electron transitions, which are from s valence electron n_s to lattice electron n_l on s orbit and from p and d valence electrons on p and d orbits to dumb-pair electron on d orbit for Tl, which induce the decrease of cohesive energy and melting point of RETl$_3$.

2.5. Co dilute RIn$_3$ (R = Gd, Nd) alloys

2.5.1. GdIn$_{3-x}$Co$_x$ ($x = 0.1,\ 0.2,\ 0.3$) alloys

Since Co and In in the GdIn$_{3-x}$Co$_x$ alloy are randomly occupations at the 3c position, a weighted average method is used to estimate the various electron numbers and single-bond radius at In crystal position based on the compositions of In and Co. According to the crystallographic data of GdIn$_{3-x}$Co$_x$,[34] the experimental bond-lengths are measured with Diamond software. The calculated and observed bond lengths and numbers of covalence electron pair of GdIn$_{3-x}$Co$_x$ ($x = 0.1$, 0.2, 0.3) are listed in Table 3. The calculated bond lengths and magnetic moments fit the experimental ones well. The number of covalence electron pair n_α is significantly affected by Co doping content, it shows that n_α decreases from 0.4005 to the range of 0.3564–0.3899 for the strong Gd–In bond, however, increases from 0.1131 to the range of 0.1691–0.1707 for In–In bond, and a little increase from 0.0037 to the range of 0.0042–0.0051 for weak Gd–Gd bond. It is suggested that Co doping into GdIn$_3$ mainly modulates the distributions of covalence electron pairs on Gd–In and In–In bonds. It is suggested that the anisotropy of distribution of covalence electron pairs on various bonds is improved by Co-dopant. The numbers of various valence electrons and single-bond radii of Co-doped Gd (In, Co)$_3$ are listed in Table 4. It is obvious that the Co doping into GdIn$_3$ modulates the valence electron structure of Gd, and causes the hybrid state translates from the 5-th to the 6-th level, which induces the increase of covalence electron numbers from 2.2921 to 2.3751, but, the decrease of lattice electron numbers from 0.7078 to 0.6248. The valence electron structure of In is independence from Co dopant. With the increase of doping content of Co, the hybrid state of Co shifts from the 14-th to the 17-th level, which causes the increase of covalent electron numbers per atom n_c/atom from 3.0867 of pure GdIn$_3$ to the range of 3.1691–3.3616 for GdIn$_{3-x}$Co$_x$ with $x = 0.1$–0.3. However, the magnetic electron number declines with increase of Co doping content, which is due to the electron transformation from 3d magnetic electron to d valence electron on 3d orbit. It means that the increase of doping content of Co is beneficial for enhancing the bonding interaction of In–In bond, but, not for increasing magnetic moment.

Table 3. The calculated and experimental bond lengths and the number of covalence electron pairs of GdIn$_{3-x}$Co$_x$ ($x = 0.1$, 0.2, 0.3).

x	Bond order	T_m (cal)	m^{3d} (cal)	m^{3d} (exp)[33]	I_α	D (Å)	$\bar{D}$ (Å) (cal)	ΔD (Å)	n_α
0.1	Gd–InCo	1496	0.3932	0.5706	24	3.2928	3.2656	0.0085	0.3564
	InCo–InCo				24	3.2928	3.2656	0.0085	0.1707
	Gd–Gd				6	4.6467	4.6162	0.0085	0.0042
0.2	Gd–InCo	1584	0.1444	0.1444	24	3.2952	3.2401	–0.0158	0.3735
	InCo–InCo				24	3.2952	3.2401	–0.0158	0.1700
	Gd–Gd				6	4.6601	4.5887	–0.0158	0.0046
0.3	Gd–InCo	1660	0.0862	0.0862	24	3.2917	3.2164	–0.0424	0.3899
	InCo–InCo				24	3.2917	3.2164	–0.0424	0.1691
	Gd–Gd				6	4.6552	4.5662	–0.0424	0.0051

Table 4. Numbers of various electrons and single-bond radii of $GdIn_{3-x}Co_x$ ($x = 0.1, 0.2, 0.3$).

x	Atom	σ	n_l	n_c	n_s	n_p	n_d	m^{3d}	$R(1)$
0.1	Gd	6	0.6249	2.3751	0.3751	0.6249	1.3751	0	1.5943
	In	9	0.3601	3.9197	0.6399	2.6399	0.6399	0	1.4004
	Co	A1 11	1.1413	5.288	0	0	5.288	1.712	1.1331
0.2	Gd	6	0.6249	2.3751	0.3751	0.6249	1.3751	0	1.5943
	In	8	0.5495	3.3516	0.4505	2.4505	0.4505	0	1.4127
	Co	A2 16	0.2889	6.5668	0.8556	2	3.7111	0.1444	1.062
0.3	Gd	6	0.6249	2.3751	0.3751	0.6249	1.3751	0	1.5943
	In	8	0.5495	3.3516	0.4505	2.4505	0.4505	0	1.4127
	Co	A2 17	0.1724	6.7414	0.9138	2	3.8276	0.0862	1.0523

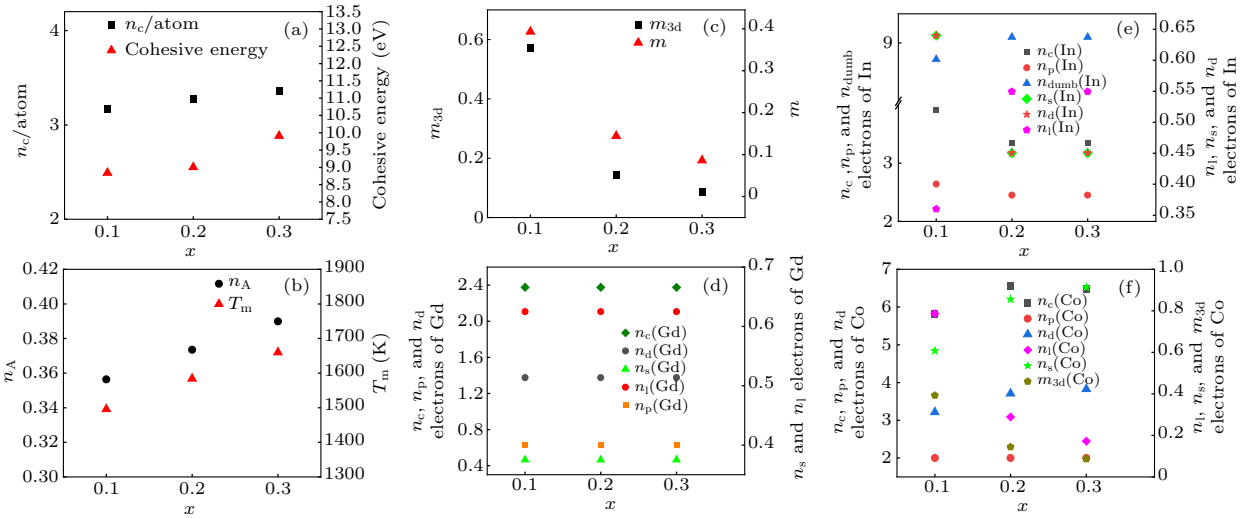


Fig. 3. The correlation of valence electron structure and melting point and cohesive energy of $GdIn_{3-x}Co_x$: (a) the cohesive energies and covalence electrons for $GdIn_{3-x}Co_x$; (b) the melting points and covalence electron pairs of $GdIn_{3-x}Co_x$; (c) the moments and magnetic electron numbers of $GdIn_{3-x}Co_x$; (d) the covalence, lattice, and s, p, d orbits electrons of Gd in $GdIn_{3-x}Co_x$; (e) the covalence, lattice, dumb-pair, and s, p, d orbits electrons of In in $GdIn_{3-x}Co_x$; (f) the covalence, lattice, dumb-pair, and s, p, d orbits electrons of Co in $GdIn_{3-x}Co_x$.

The thermal and magnetic properties of cobalt doped $GdIn_3$ are strongly related to their valence electron structures, as shown in Figs. 3(a)–3(c). The correlation of thermal properties and valence electron structures is very similar to the REX_3 one. The cohesive energy depends upon the covalence electron number n_c, and raises with the increase of n_c, as shown in Fig. 3(a). The melting point is proportional to the number of maximum covalence electron pair n_A, as shown in Fig. 3(b). The changes of various electrons are shown in Figs. 3(d)–3(f), the change tendency of covalence electron number is reversal to those of lattice and 3d magnetic electrons with increase of Co doping contents, it means that Co doping into $GdIn_3$ drives the electron transforms from lattice and 3d magnetic electrons to covalence electron. Figure 3(c) shows that magnetic moment is strongly affected by 3d magnetic electron number. The minor amount of Co doping into $GdIn_3$ causes room temperature ferromagnetic characteristics, which is due to the exchange coupling interaction by introducing 3d magnetic electron of Co on In–In bond. However, the moment is weakened with increase of Co doping content due to the electron transformation from 3d magnetic electron to d valence electron on 3d orbit. It reveals that ferromagnetic characteristics is originated from the minor cobalt diluted in $GdIn_3$, but, not doping more content of Co. In addition, the lattice electron decreases with increase of Co doping content, which weakens the electric conducting property, and induces the electric phase transformation from metal conductor to half-metal state. Thus, it is suggested the nature of cobalt diluted $GdIn_3$ alloy is ferromagnetic half-metal.

2.5.2. $NdIn_{3-x}Co_x$ ($x = 0.1,\ 0.2,\ 0.3$) intermetallic compounds

The cobalt dilute $NdIn_{3-x}Co_x$ ($x = 0.1$–0.3) alloys are also experimentally conformed to be a single-phase solid solution of $NdIn_3$. The calculated and observed bond lengths and numbers of covalence electron pairs of $NdIn_{3-x}Co_x$ ($x = 0.1$–0.3) are listed in Table 5. The calculated bond lengths and magnetic moment agree with the observed ones measured according to the crystallographic ordinates of $NdIn_{3-x}Co_x$ ($x = 0.1$–0.3).[34] The distribution of covalence electron pairs of cobalt dilute $NdIn_3$ are very similar to those of $GdIn_{3-x}Co_x$ ($x = 0.1$–0.3). Co doping into $NdIn_3$ significantly modulates the distribution of covalence electron pairs n_α on various bonds, and improves the anisotropy of distribution of n_α. It shows that the numbers of covalence electron pair n_α decreases significantly from 0.4109 to the range of 0.3580–0.3924 on the strongest Nd–In bond, but, increases from 0.1025 to the range of 0.1537–0.1688 for In–In bond, and a very little increase from 0.0041 to the range of 0.0050–0.0053

for weak Nd–Nd bond. Table 6 lists the numbers of various valence electrons and single-bond radii of $NdIn_{3-x}Co_x$. It can be seen that the modulation of Co dopant on the valence electron structure of Nd is different from that of Gd, the small amount of Co doping content ($x \leq 0.1$) does not affect the valence structures of Nd and In. With the increase of Co doping content ($x > 0.1$), the modulation of Co on Nd is the same as that of Gd. The hybrid state of Nd translates from 5-th to 6-th level with increase of covalence electron numbers from 2.2921 to 2.3751 and the decrease of lattice electron numbers from 0.7078 to 0.6248, however, the valence electron structure of In does not change. With the increase of doping content of Co, the hybrid state of Co translates from the 16-th to 12-th level, which causes the increase of covalent electron numbers per atom n_c/atom from 3.0867 of pure $NdIn_3$ to the range of 3.1671–3.2846 for $NdIn_{3-x}Co_x$ with $x = 0.1$–0.3. However, the numbers of 3d magnetic electrons of Co show a reversal change comparing to that of Co doping into $GdIn_3$, the magnetic electron number raises from 0.4333 to 1.2855 with increasing Co doping content from $x = 0.1$ to 0.3, which is due to the electron transformation from d valence electron to 3d magnetic electron on 3d orbit, the number of lattice electron raises with increase of Co doping content, which can enhance the electric conducting property, and induces the ferromagnetic-metal state.

Table 5. The valence bond lengths of $NdIn_{3-x}Co_x$ ($x = 0.1, 0.2, 0.3$) compounds.

x	Bond order	T_m (cal)	m^{3d} (cal)	m^{3d} (exp)[33]	I_α	D (Å)	$\bar{D}$ (Å)	ΔD (Å)	n_α
0.1	Nd–InCo				24	3.2928	3.2658	–0.0270	0.3580
	InCo–InCo	1672	0.4190	0.4333	24	3.2928	3.2658	–0.0270	0.1688
	Nd–Nd				6	4.6467	4.6297	–0.0270	0.0040
0.2	Nd–InCo				24	3.2952	3.2667	–0.0285	0.3841
	InCo–InCo	1748	0.9730	0.8858	24	3.2952	3.2667	–0.0285	0.1555
	Nd–Nd				6	4.6601	4.6316	–0.0285	0.0050
0.3	Nd–InCo				24	3.2917	3.2526	–0.0390	0.3924
	InCo–InCo	1772	1.5390	1.2858	24	3.2917	3.2526	–0.0390	0.1537
	Nd–Nd				6	4.6552	4.6161	–0.0390	0.0053

Table 6. Valence electron structures of $NdIn_{3-x}Co_x$ ($x = 0.1, 0.2, 0.3$) compounds.

x	Atom	σ	n_l	n_c	n_s	n_p	n_d	m^{3d}	$R(1)$
0.1	Nd	5	0.7078	2.2921	0.2921	0.7078	1.2921	0	1.5970
	In	8	0.5494	3.3515	0.4505	2.4505	0.4505	0	1.4127
	Co	A1 16	0.2888	6.5666	0	0	6.5666	0.4333	1.0621
0.2	Nd	6	0.6248	2.3751	0.3751	0.6248	1.3751	0	1.5943
	In	8	0.5494	3.3515	0.4505	2.4505	0.4505	0	1.4127
	Co	A1 15	0.5905	6.1141	0	0	6.1141	0.8858	1.0872
0.3	Nd	6	0.6248	2.3751	0.3751	0.6248	1.3751	0	1.5943
	In	8	0.5494	3.3515	0.4505	2.4505	0.4505	0	1.4127
	Co	A1 12	0.8570	5.7144	0	0	5.7144	1.2855	1.1094

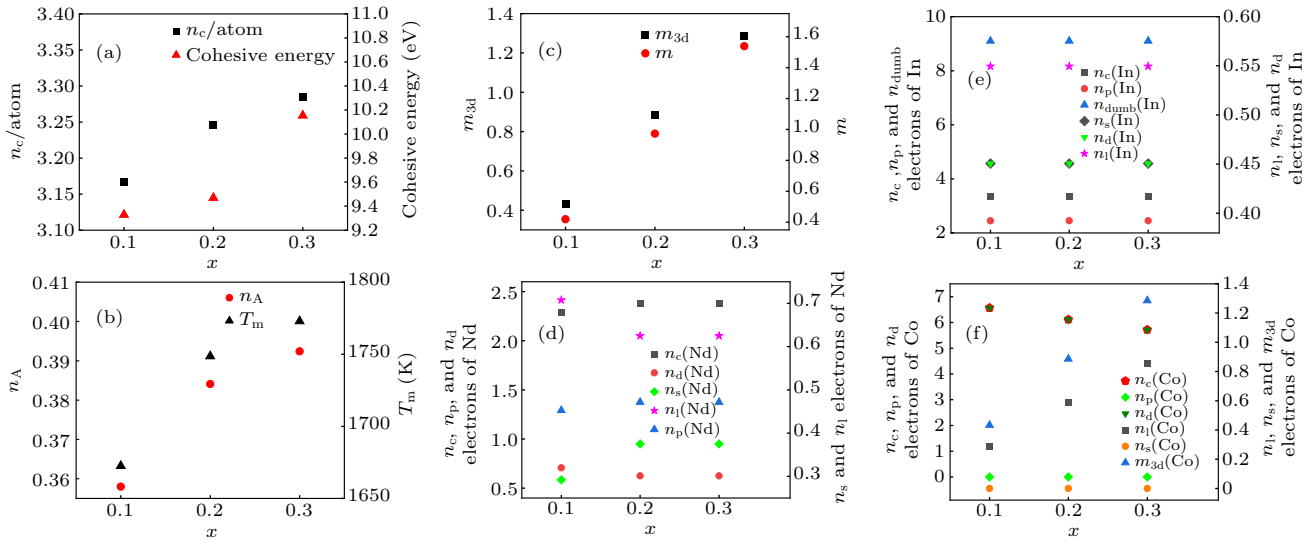


Fig. 4. The correlation of valence electron structure and melting point and cohesive energy of $NdIn_{3-x}Co_x$: (a) the cohesive energies and covalence electrons for $NdIn_{3-x}Co_x$; (b) the melting points and covalence electron pairs of $NdIn_{3-x}Co_x$; (c) the moments and magnetic electron numbers of $NdIn_{3-x}Co_x$4; (d) the covalence, lattice, and s, p, d orbits electrons of Nd in $NdIn_{3-x}Co_x$; (e) the covalence, lattice, dumb-pair, and s, p, d orbits electrons of In in $NdIn_{3-x}Co_x$; (f) the covalence, lattice, dumb-pair, and s, p, d orbits electrons of Co in $NdIn_{3-x}Co_x$.

The cohesive energy is related to the covalence electron number n_c, and shows proportional to n_c, as shown in Fig. 4(a). The melting point is proportional to the number of maximum covalence electron pair n_A, as shown in Fig. 4(b). Figure 4(c) shows that the moment originates from the 3d magnetic electron, the changes of various electrons of Co are shown in Figs. 4(d)–4(f), the change tendency of number of lattice electron is similar to that of 3d magnetic electrons with increase of Co doping contents, however, the number of d valence electrons shows a reversal tendency, it can be explained by the electron transforms from d valence electron to 3d magnetic electrons and lattice electron.

3. Conclusion and perspectives

EET has been used to study the valence electronic structures, melting points, cohesive energies, and magnetic moments of REX_3 intermetallic compounds and cobalt diluted $RE(\mathrm{In,Co})_3$ alloys. The calculated bond lengths and moment are in good agreement with the experimental ones. The study reveals that structural stability and physical properties of REX_3 and their cobalt dilute alloys are strongly related to their valence electron structures modulated by shrinking effect of single-bond radius $R(1)$ for RE. With the decrease of single–bond radius, the overlap ability of electron cloudy β lightly increases, which is helpful for enhancing the overlap ability of electron cloudy. The large decrease of $R(1)$ of heavy rare earth causes the electron transformation from valence electron to lattice electron, and induces a reversal electron transformations from lattice electron to valence electron associated with an additional transition from dumb-pair electron to valence electron for In. The cohesive energy strongly depends upon the covalence electron n_c, and arise with the increase of n_c. Since the high cohesive energy is beneficial for the structural stability, it is suggested that increase of n_c can stabilize the crystal structure. The melting point is strong relative to the maximum number of covalence electron pair n_A, and increases with n_A. The ferromagnetic characteristics of Co diluted $RE\mathrm{In}_3$ alloys is originated from the introduction of strong ferromagnetic Co atom, and the moment is strongly related to the numbers of 3d magnetic electrons of Co. However, there is a competition of mutual electron transformations between d valence electron and magnetic electron induced by doping more contents of Co. For Co-diluted GdIn_3 alloy, the moment is weakened with increase of Co-doping content due to the electron transformation from 3d magnetic electron to d valence electron on 3d orbit. It reveals that strong ferromagnetic characteristics is originated from the minor amount of cobalt doping into GdIn_3, but, not more doping content of Co. In addition, the lattice electron decreases with increase of Co doping content, which causes the weakening effect of electric conducting property, and induces the electric phase transformation from metal conductor to half-metal state. Thus, it is suggested the nature of cobalt diluted GdIn_3 alloy is ferromagnetic half-metal.

In the case of Co-diluted NdIn_3, the numbers of 3d magnetic electrons of Co shows a reversal change comparing to that of Co-doped GdIn_3. The magnetic electron number raises due to the electron transformation from d valence electron to 3d magnetic electron on 3d orbit, and the number of lattice electron raises with the increase of Co doping content, which can enhance the electric conducting property, and induces a ferromagnetic-metal state.

References

[1] Kletowski Z 1992 *Solid State Commun.* **83** 241
[2] Settai R, Kubo T, Matsuda T D, Haga Y, Ōnuki Y and Harima H 2006 *Physica B* **378–380** 417
[3] Kletowski Z, Fabrowski R, Slawiński P and Henkie Z 1997 *J. Magn. Magn. Mater.* **166** 361
[4] Kletowski Z, Czopnik A, Tal A and De Boer F 2000 *Physica B* **281–282** 163
[5] Umehara I, Ebihara T, Nagai N, Fujimaki Y, Satoh K and Ōnuki Y 1992 *J. Phys. Soc. Jpn.* **61** 19
[6] Hale L, Gschneidner K A, Pecharsky V K and Mudryk Y 2009 *J. Alloys Compd.* **472** 24
[7] Cabrera-Pasca G A, Mestnik-Filho J, Carbonari A W and Saxena R N 2013 *J. Appl. Phys.* **113** 17
[8] Silva L S, Peixoto E B, Mercena S G, Coelho A A, Meneses C T and Duque J G S 2016 *Mater. Lett.* **175** 9
[9] Silva L S, Peixoto E B, Mercena S G, Coelho A A, Meneses C T and Duque J G S 2016 *J. Supercond. Nov. Magn.* **29** 423
[10] Wang C, Guo Y Q and Yang S W 2019 *Chin. Phys. B* **28** 086101
[11] Fulfer B W, McAlpin J D, Engelkemier J, McCandless G T, Prestigiacomo J, Stadler S, Fredrickson D C and Chan J Y 2014 *Chem. Mater.* **26** 1170
[12] Guo Y, Grin Y, Schnelle W and Li W 2007 *J. Appl. Phys.* **101** 09N505
[13] Chen S, Guo Y and He Q 2015 *J. Appl. Phys.* **117** 123910
[14] De Negri S, Kaczorowski D, Grytsiv A, Alleno E, Giovannini M, Gorzelniak R, Rogl P, Godart C, Saccone A and Ferro R 2004 *J. Alloys Compd.* **365** 58
[15] Singh S, Dhar S K, Manfrinetti P and Palenzona A 2002 *J. Magn. Magn. Mater.* **250** 190
[16] Dhar S K, Manfrinetti P and Palenzona A 2002 *Solid State Commun.* **124** 379
[17] Liu Y S, Sun H, Hu C S, Wu Y J and Zhang C W 2023 *Chin. Phys. B* **32** 027101
[18] Nie Y, Tang G, Li Y, Zhang M and Zhao X 2024 *Chin. Phys. B* **33** 047301
[19] Chen Q, Wu J, Chen T, Wang X, Ding C, Huang T, Lu Q and Sun J 2022 *Chin. Phys. B* **31** 056201
[20] Antonov V N 2014 *Low Temp. Phys.* **40** 297
[21] Asadabadi S J and Akbarzadeh H 2004 *Physica B* **349** 76
[22] Betsuyaku K and Harima H 2004 *J. Magn. Magn. Mater.* **272–276** 1005
[23] BabanlıA M and Ibragimov B G 2017 *Superlattices Microstruct.* **111** 574
[24] Guo X P, Guo Y Q and Yin L H 2021 *J. Phys. Chem. C* **125** 20503
[25] Guo Y, Su T, Zhang J, Wang X, Chen Y and Zhao X 2020 *ACS Appl. Energy Mater.* **3** 5361
[26] Guo Y, Yü R, Zhang R, Zhang X and Tao K 1998 *J. Phys. Chem. B* **102** 9
[27] Wang T, Guo Y Q and Li S 2017 *Chin. Phys. B* **26** 103101
[28] Xue Z Q and Guo Y Q 2016 *Chin. Phys. B* **25** 063101
[29] Yin L, Guo Y and Guo X 2022 *Inorg. Chem.* **61** 2402
[30] Wang T, Guo Y Q and Wang C 2021 *Chin. Phys. B* **30** 043101
[31] Anon 1981 *Acta Crystallogr. Sect. A* **37** 144
[32] Yatsenko S P, Semyannikov A A, Shakarov H O and Fedorova E G 1983 *J. Common Met.* **90** 95
[33] Saccone A, Delfino S and Ferro R 1988 *J. Common Met.* **143** 1
[34] He Q 2016 *Structural stability and Dilute magnetic effect of Minor Co-doped Rare-Earth In-based 1:3 Compounds*, MS dissertation (Beijing: North China Electric Power University (Beijing))